SEPARATION CONTROL USING AIR-JET VORTEX GENERATORS IN A HYPERSONIC SHOCK-INDUCED BOUNDARY-LAYER SEPARATION

D.P. Ramaswamy*, A. Barklage†, A-.M. Schreyer*
* Institute of Aerodynamics, RWTH Aachen University, Aachen, Germany
† Institute of Fluid Mechanics, TU Braunschweig, Braunschweig. Germany

Abstract

An experimental analysis was carried out to assess the flow organisation and control effectiveness of an array of air-jet vortex generators (AJVGs) on an axisymmetric 33^o flare induced shock-wave/boundary layer interaction at Mach 5.15. This is the first study of AJVGs in a hypersonic shock-wave/boundary layer interaction. Flow configurations for three different Reynolds numbers (Re_∞) and various momentum-flux ratios (J) were investigated using schlieren and surface oil-flow visualisations. The jets have a diameter of 1mm and are pitched at 45^o with respect to the local surface tangent, resulting in a purely azimuthal injection. Well defined separation and reattachment shocks were captured in the uncontrolled baseline configuration for all tested Reynolds numbers with minimal variation in their structure. Upon jet-injection, asymmetric pairs of counter rotating vortices are generated, which alter the structure of the boundary layer and the separation shock. Only a weak influence of air-jet vortex generators was seen at low momentum-flux ratios and flow Reynolds numbers. At higher values of J and Re_∞, the jets represent a large obstruction, resulting in even earlier flow separation than in the uncontrolled case. This rather unexpected result may be related to the axisymmetry of the flow field.

Keywords
air-jet vortex generators; hypersonic shock-wave/boundary-layer interaction; flow control

NOMENCLATURE

Formelzeichen

δ	boundary layer thickness	mm
ϕ	jet-pitch angle	deg
ρ	density	kg/m^3
θ	jet-skew angle	deg
D	spacing between the jet-orifices	mm
d_{jet}	jet-orifice diameter	mm
J	momentum flux ratio	deg
M	Mach Number	
P	pressure	Pa
Re	unit Reynolds number	m^{-1}
T	temperature	K
U	Streamwise velocity	m/s

Indizes

∞	freestream properties
e	boundary layer edge properties
o	stagnation properties

Abkürzungen

AJVG	air-jet vortex generators
SWTBLI	shock-wave turbulent boundary layer interaction

1. INTRODUCTION

Hypersonic aircraft and re-entry vehicles are susceptible to shock-wave/turbulent-boundary-layer interactions (SWTBLI) which can have drastic consequences on the structure and operation of the vehicle [1]. Strong shock waves induced by surface discontinuities, control-surface deflections etc., can impose large adverse pressure gradients on the incoming boundary layer and can lead to large-scale local flow separation. Separated flows are strongly detrimental and can lead to a loss in control-surface effectiveness or scramjet air-intake effectiveness, amongst other effects. The associated aerothermodynamic loads on the vehicle surface pose an immense challenge for thermal protective systems. Additionally, such interactions are characterised by low-frequency oscillations of the shock/separation-bubble system [2] and impart unsteady fluctuating pressure loads that can lead to severe structural damage. A multitude of studies on SWTBLIs in 2D and 3D configurations have been carried out to better understand the structure and

doi:10.25967/530277

governing mechanisms, which have been compiled and discussed in several review articles [1–5].

To ensure safe and reliable operation of the vehicle and enable smarter vehicle designs, proper control of separated interactions is crucial [6]. Hence, several flow control strategies were employed, which have helped reduce the drastic effects of shock-induced boundary-layer separation. One commonly studied approach is based on altering the incoming boundary-layer characteristics using mechanical micro-vortex generators, constituting of low-profile vanes or ramps with heights between 10% and 50% of the boundary-layer-thickness (δ) [7, 8]. The flow topology and control effectiveness, especially of sub-boundary layer micro-ramps, has been a topic of extensive study in the past few decades [8–13]. These devices generate streamwise vortices downstream of their installation which redistribute the momentum within the boundary layer and make the boundary layer more resistant to separation. However, they are usually designed and optimised for a particular flight condition and cannot be turned off when not needed and hence suffer from parasitic drag under all flight conditions. An alternative method to mitigate flow separation is by using air-jet vortex generators (AJVGs), introduced by Wallis [14]. Here, streamwise vortices are induced by steady air-jets injected into the crossflow [15, 16]. Preliminary investigations of AJVGs [7, 14, 17] showed that their effectiveness is comparable to that of mechanical vortex generators.

Air-jet vortex generators have a number of design parameters that influence the topology of the induced vortex structures and their effectiveness in mitigating shock-induced separation. In an attempt to identify an optimised and effective configuration, a number of parametric studies have been carried out. Investigations on the jet-orifice diameter [18] have shown that AJVGs with small orifices of less than 0.25δ are more effective in mitigating flow separation. Investigations on jet-orientation have shown that jet arrays with spanwise-inclined jets perform better and that no streamwise jet component is required [14, 15, 19, 20]. This effect is a result of the sustained low jet-penetration depth [21]. Ramaswamy et. al. [22] and Verma and Manishankar [23] investigated the effect of jet spacing within AJVG arrays, and revealed that an adequate amount of interaction between the jet-induced streamwise vortices is essential for effective flow control. Szwaba [15] showed that low injection pressures of the order of work best for separation control purposes; this behavior is most probably related to similar interactions between the jet-induced vortex structures as observed for the most favorable jet spacing [22]. In addition to the achieved decrease of the separation bubble, AJVGs also effectively reduce the unsteadiness of the shock/separation bubble system [20].

Almost all investigations discussed above were carried out in the transonic and supersonic flow regimes, where the effectiveness of air-jet vortex generators in mitigating shock-induced flow separations have already been verified. With the renewed interest in the development of sustainable hypersonic transport vehicles, studies on flow control strategies and their effectiveness should be extended to high Mach number flows. However, in comparison to the subsonic, transonic, and supersonic flight regimes, investigations of separation control in hypersonic flows are rather scarce. Experimental [11, 12] and computational [24–26] analyses have been performed to better understand a hypersonic shock-wave/boundary layer interaction controlled by micro-ramp vortex generators; no such studies exist for AJVG-controlled interactions so far (to the author's knowledge). In addition to the advantages discussed earlier, air-jet vortex generators are of particular interest in hypersonic flow regimes, since they offer the potential to combine separation control and film cooling (see for e.g. Szwaba et. al. [27]). Hence, to gain a better understanding of the flow topology and control mechanism in hypersonics flow, we conducted an experimental investigation on an axisymmetric 33^o flare-induced hypersonic shock-wave/boundary-layer interaction using flow visualisation tools. This is a first study of AJVG-controlled shock-wave/boundary-layer interactions in the hypersonic flow regime.

2. EXPERIMENTAL SETUP

2.1. Flow facility

The experiments for this investigation were conducted in the Hypersonic Ludwieg tube (HLB) at the Technische Universität Braunschweig (see Fig 1). It is based on the Ludwieg-tube concept and consists of a 17 m long high-pressure storage tube with a max. capacity of 30 bars which is separated from the wind tunnel nozzle, the evacuated test section and the vacuum dump tank ($< 6mbar$) via a fast-acting pneumatic valve and a de Lavel nozzle. The first $3m$ of the high-pressure storage tube are heated up to $\sim 500K$ to avoid condensation effects. Upon operating the fast-acting valve, the hot air in the storage tube expands and accelerates to Mach 5.9 in the test section. The total test time of 80 ms is given by the time of the expansion wave generated at the valve to travel downstream where it gets reflected at the storage tube end and then reaching again the valve. The total temperature and total pressure in the storage tube are monitored using a pressure transducer and a thermocouple. The freestream unit Reynolds number can be controlled by adjusting the total pressure in the storage tube. Three circular quartz windows provide optical access to the circular test section ($0.5m$ in diameter). Further details on the wind tunnel operation and uncertainty characterisation can be found in Estorf et al. [28] and Ali et al. [29].

2.2. Wind-tunnel model and investigated cases

The axisymmetric wind tunnel model consists of a 25^o cone in the front, followed by a 186 mm long cylin-

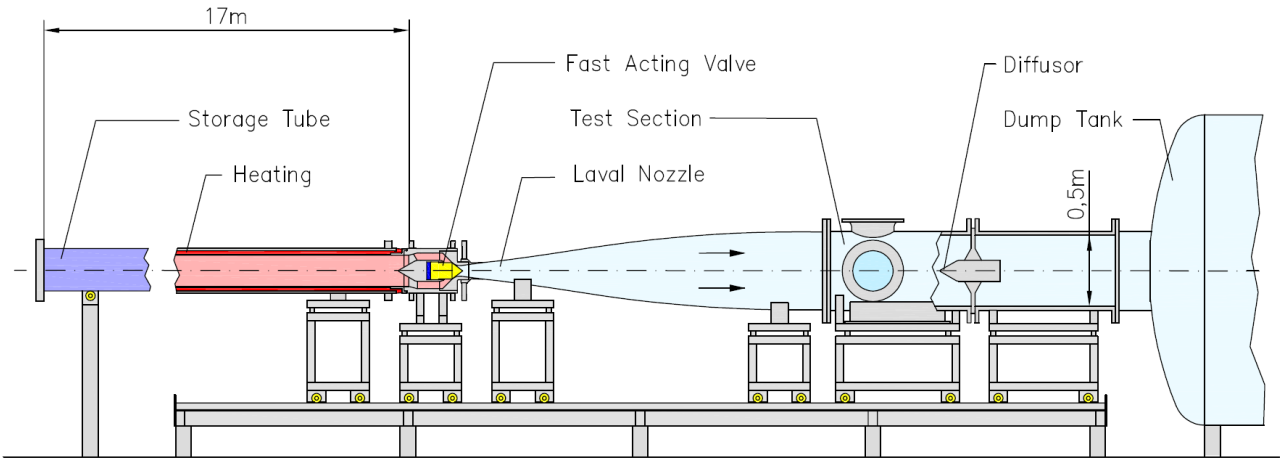

FIG 1. Schematic of the HLB

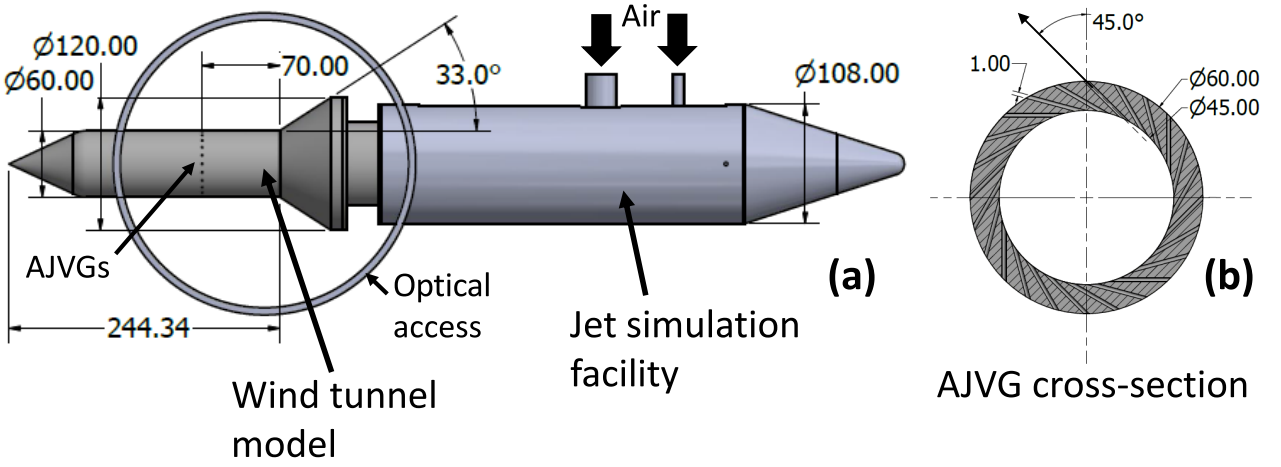

FIG 2. (a) Schematic of the wind tunnel model secured to the jet-simulation facility. Flow is from left to right. (b) Cross-section view of the AJVGs.

drical body and a 33^o flare with a surface length of 55 mm (see Fig 2a). A roughness strip of approximately 1 mm height was placed 18 mm downstream of the cone leading edge to force transition of the incoming boundary layer. The incoming flow undergoes compression due to the presence of the conical shock induced by the 25^o front-cone. The conditions downstream of the conical shock are obtained by solving the Taylor-Maccoll equations (see Anderson [30]). Subsequently, the flow undergoes Prandtl-Meyer expansion at the expansion corner at the junction between the nose cone and the cylindrical body and the boundary layer starts developing on the axisymmetric cylindrical surface. 186 mm downstream of the expansion corner is the cylinder/flare interface. Two separate cylindrical sections were manufactured for the baseline and control cases, respectively. To study the influence of control, AJVGs were placed on the second cylindrical model at 70 mm ($\approx 14\delta$) upstream of the cylinder-flare interface. The AJVG array consists of a single row of 24 circular orifices of $d_{jet} = 1$ mm diameter, drilled in the configuration depicted in the sectional view in Fig 2. The jets are pitched at an angle of 45^o to the local surface tangent, resulting in a purely azimuthal injection. The wind tunnel model is attached firmly to the jet simulation facility (TSA) [31], which provides air supply for the air-jet vortex generators. The working principle of the TSA is similar to the Hypersonic Ludweig Tube. A pair of control valves operate the jet simulation facility and both the HLB and the TSA were synchronised to run simultaneously. However, this operation mode restricts the minimum injection pressure of the AJVGs to $1bar$ (atmospheric pressure). In order to achieve lower injection pressures, the first throat of the TSA was removed and the TSA's control value was modified and reprogrammed. The TSA is secured to the upper wall of the test section via an aerodynamic strut support. A detailed description of the unmodified TSA can be found in Stephan and Radespiel [31]. The Mach number downstream of the conical shock and the subsequent expansion wave is equal to $M_e = 5.15$.

Three different flow Reynolds number were tested to gain an understanding of their effect on the control effectiveness: (a) $Re_\infty = 9 \times 10^6 m^{-1}$, (b) $Re_\infty = 10 \times 10^6 m^{-1}$, (c) $Re_\infty = 11.5 \times 10^6 m^{-1}$. The corresponding momentum thickness based Reynolds number (Re_θ) obtained from the approximate analytical expressions of Stratford and Beavers [32] equals (a) $Re_\theta = 1600$, (b) $Re_\theta = 1750$ and (c) $Re_\theta = 1950$,

respectively. Additionally, at each Re_∞, a number of AJVG injection pressures, and hence momentum flux ratios were tested in an attempt to find appropriate injection conditions. The tested configurations are listed in Tab. 1.

TAB 1. Tested configurations

CASE	P_{os} [bar]	P_{oj} [bar]	Re_∞ $[m^{-1}]$	F	J
Baseline	6.45	-	9×10^6	-	-
	7.3	-	10×10^6	-	-
	8.5	-	11.5×10^6	-	-
Control	6.45	0.36	9×10^6	1.9	0.7
		0.52		2.8	1.0
		0.70		3.7	1.3
		2.60		14.1	5.0
	7.3	0.38	10×10^6	1.8	0.6
		0.47		2.2	0.8
		0.59		2.8	1.0
		0.88		4.1	1.5
		1.05		4.9	1.7
		2.60		12.0	4.3
	8.5	0.53	11.5×10^6	2.1	0.8
		0.64		2.6	1.0
		0.85		3.5	1.3
		0.93		3.8	1.4
		1.20		4.9	1.8
		2.70		11.1	3.9

The mass flux ratio (F) and the momentum flux ratio is defined as:

$$F = \frac{\rho_j V_j}{\rho_\infty V_\infty} \tag{1}$$

$$J = \frac{\gamma p_j {M_j}^2}{\gamma p_e {M_e}^2} \tag{2}$$

The flow Reynolds number was modified by changing the storage-tube pressures and the momentum flux ratio was adapted by controlling the jet-simulation facility's supply pressure.

2.3. Experimental techniques

To obtain an overview of the influence of several parameters and a range of their values on AJVG control in hypersonic SWTBLI, we primarily employed flow visualisation tools to assess the flow organisation of the baseline and the AJVG-controlled interactions. In particular, the effects of jet momentum-flux ratio and Reynolds number are investigated (see Tab. 1), and in comparison with previous studies, potential effects of Mach number and model axisymmetry are discussed. The density gradients were characterised using a single-mirror coincident schlieren arrangement. The

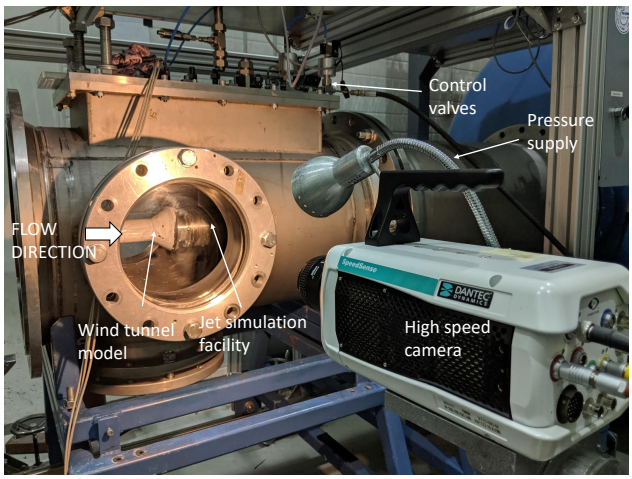

FIG 3. Set-up of the oil-flow visualisation

image sequences were recorded at 20kHz using a Phantom v711 high speed camera at $640px \times 480px$, resulting in a digital resolution of $4.6px/mm$. A horizontal knife edge was used.
Additionally, the surface flow features were visualised using an oil-flow visualisation technique. In low-speed wind tunnels, the oil-film approach is fairly straightforward and enjoys the benefit of long run times. The HLB operation time, however, is in the range of milliseconds and hence, visualisations using the oil-flow technique can be challenging. For this analysis, an oil-mixture consisting of hydraulic oil, Titanium dioxide particles, and oelic acid was used. The exact proportions were narrowed down after an extensive preliminary test campaign. However, the low surface shear stress and short test times meant that the movement of oil in the flat cylindrical part of the wind tunnel model was minuscule in comparison to the movement of oil along the flare surface, where the oil is susceptible to a much larger surface shear stress. Moreover, the abrupt shut-off of the fast acting valve of the wind tunnel completely impairs the oil patterns developed during the steady state flow. Thus, in order to capture the transient oil-flow pattern, the Phantom v711 high speed camera was employed at $7.5kHz$ to record visualisation images. By tracing the oil-movement during the $80ms$ operation time of the facility, we ensure the accurate extraction of the flow features. Fig 3 shows the setup of the oil-flow visualisations. The oil-mixture was applied on the cylindrical and flare surface before evacuating the test section and the vacuum dump tank using a kitchen sponge.

3. RESULT AND DISCUSSION

In this section, the results of the schlieren and oil-flow visualisation campaigns will be presented and discussed.

3.1. Baseline shock-wave/boundary-layer interaction:

Fig 4 shows the mean schlieren images of the uncontrolled interaction at three flow Reynolds number. The

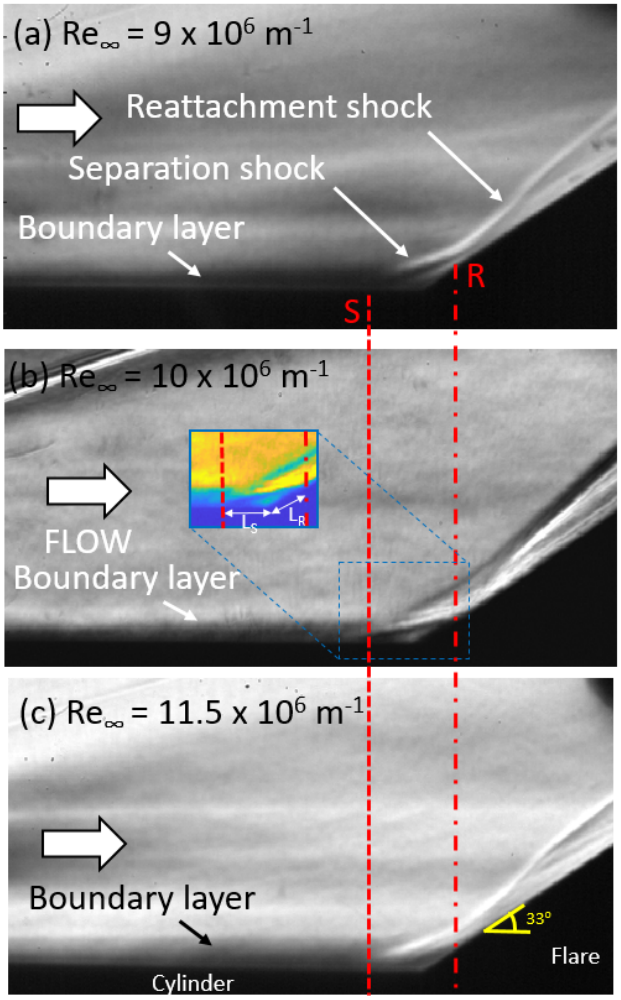

FIG 4. Mean Schlieren visualisation of the baseline interaction at three Reynolds number. S - Separation point; R - Reattachment point. The RMS of mean-subtracted intensity colourmap in (b) shows the recirculation region.

mean images were obtained by averaging about 50 instantaneous schlieren frames. The typical characteristics of a shock-induced separation are clearly captured. The boundary layer is seen to develop on the surface of the cylinder and is visible as a dark patch close to the walls of the cylinder. However, a clear distinction between the boundary layer and the freestream is imperceptible due to the axisymmetric nature of the model that lacks the advantage of spanwise-integration of the gradients. Similar weak boundary layer features were also observed by other studies on bodies of revolution [33]. As the boundary layer approaches the cylinder/flare interface, the strong adverse pressure gradients force the boundary layer to separate (S), leading to the formation of the separation shock. The separated shear layer impinges strongly on the flare surface and a reattachment shock ensures that the flow is now aligned along the flare surface. The subfigure in Fig 4b, shows the root-mean-square of the mean-subtracted image intensities, where the flow separation and its reattachment on the flare surface is clearly identifiable. A large separation bubble ensues. As can be seen in Fig 4, changing the flow Reynolds number has minuscule influence on the overall structure of the interaction, consistent with other studies in literature [34]. On average, the total separation length of the baseline interaction ($L_S + L_R$) is $\sim 21 d_{jet}$.

3.2. Effect of AJVG control:

The global flow topology (left) and the surface-feature organisation (right) of an exemplary AJVG-controlled shock-wave/boundary-layer interaction are shown in Fig 5. The flow features of the controlled interaction in this axisymmetric configuration are very similar to its 2D planar counterpart, which is described in detail by Ramaswamy et. al. [22].

Upon injection, the air-jets impose an obstruction to the incoming flow, which results in the formation of a jet-induced shock wave and a corresponding small-scale separation upstream of the injected air jets. Due to the spanwise inclination of the injected jets, the jet-induced separation is asymmetric, with a larger separation in the direction of jet-injection [21]. The interaction of the jets with the crossflow leads to the formation of a pair of asymmetric counter-rotating vortices [21]. The footprint of the streamwise vortices can be seen as streaks in oil film in Fig 5b. The system of streamwise vortices generated by the air-jet vortex generators results in the formation of azimuthally alternating regions of low and high velocities and leads to the accumulation or dispersion of the oil-film, thereby generating the streaky pattern. The movement of the oil-film during the steady state operation of the HLB is blocked by the strong pressure gradients imposed by the separation shock. The resulting accumulation of oil helps to identify the separation line. Due to the azimuthal alteration of the boundary layer velocities, the previously 2D separation line (in the baseline case) is corrugated under the influence of control.

As the flow separates and reattaches on the flare surface, a closed recirculation region is formed. The surface oil-flow pattern depicts a point on the flare surface from which the streamlines diverge both the upstream and the downstream directions (see schematic in Fig 5b). This enables identification of the flow reattachment point from the transient oil-flow movie. Furthermore, the large flow turning angle at the cylinder/flare interface leads to centrifugal instabilities and consequently formed Görtler vortices [35], which, in combination with the jet-induced vortices, result in the formation of periodic streaks on the flare surface.

3.3. Effect of injection condition:

Studies on jet-injection pressure of AJVGs [15, 22] in low Mach number supersonic and transonic interactions have shown that good control effectiveness was achieved for air-jet injection pressures equal to the wind tunnel stagnation pressure. This choice might not be suitable for the present study, however, due to the strong expansion necessary to achieve a high Mach number in the HLB facility. This condition, in addi-

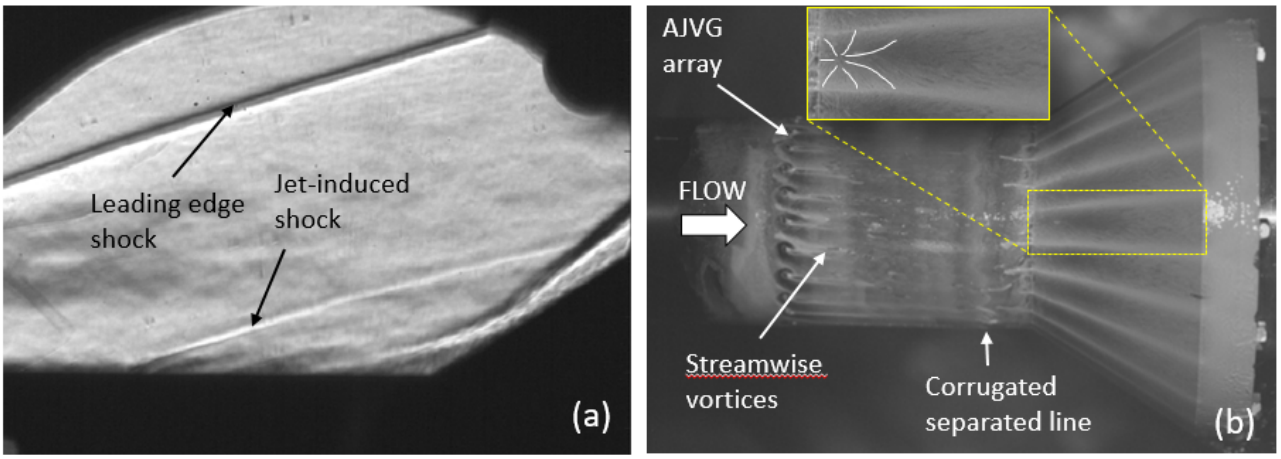

FIG 5. Effect of AJVG control. $Re_\infty = 11.5 \times 10^6 m^{-1}; J = 1$. The rectangular cut-out shows a zoom view of the reattachment region and the while likes depict the surface streamline pattern.

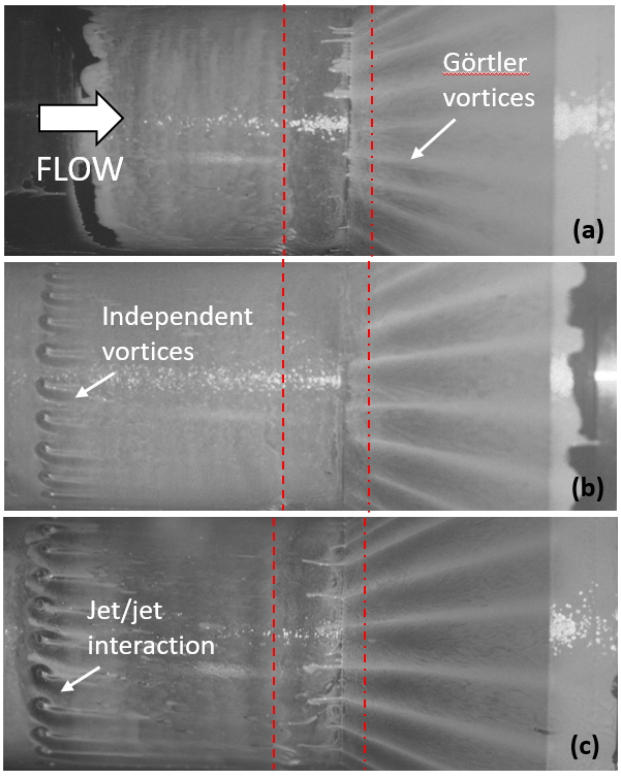

FIG 6. Oil-flow visualisation of the (a) Baseline case and AJVG injection cases with (b) $J = 0.5$ and (c) $J = 1$. $Re_\infty = 11.5 \times 10^6 m^{-1}$ for all cases.

tion to the fact that the boundary layer thickness is relatively small (~ 5 mm), means that the flow will be completely separated upstream of the AJVGs, if they are operated with $Po_{jet} = Po_e$. Hence, for this analysis, the jet-to-mainflow momentum flux ratio (J) is used for characterisation, which was also widely used in jet-in-crossflow studies in literature (see e.g. [36]). Fig 6 shows the effect of AJVGs for two selected jet-to-mainflow momentum flux ratios. The baseline oil-flow visualisation is also shown for comparison. At low values of J (Fig 6 (b)), the interactions between the individual jets are rather weak. Independent pairs of counter rotating vortices are generated by each of the 24 AJVG orifices. Due to the lack of interaction between the AJVG-induced vortices, the change in separation and reattachment lengths is negligible and the interaction is hardly altered. Doubling the momentum-flux ratio J increases the jet/jet interactions downstream of the AJVG arrays (Fig 6 (c)). Ramswamy et al. [22] and Verma and Manisankar [23] have shown the necessity of a suitable degree of jet/jet interactions for effective AJVG-control arrays in 2D interactions. In the present axisymmetric case, however, the interaction is only modified to a minor degree, in contrast to a nearly $O(\delta)$ change in separation length under similar control conditions for 2D interactions. We suspect that this behavior is not an effect of Mach number, but is related to the 3D relieving effects of the vortices on the axisymmetric cylindrical surface that might accelerate the weakening of the control effect. Reasons for our assumption are previous observations in a) microramp-separation control, where very similar effects and control efficiency has been observed in supersonic and hypersonic flows [11], and b) separation control downstream of backward-facing steps with lobe mixers, where the control effect was much weaker on an axismmetric model than on a nominally 2D configuration [37]. A further increase in momentum-flux ratio in an attempt to generate stronger vortices, dramatically increases the obstruction component of the jets and results in an upstream movement of the separation shock, worsening the shock-induced separation (image not shown).

3.4. Effect of flow Reynolds number:

In addition to the influence of the injection conditions, the effect of flow Reynolds number on the effectiveness of air-jet vortex generators was assessed and the results for $J = 1$ are shown in Fig 7. Red dash and dash-dot lines mark the separation and reattachment locations, respectively. The structures of the shock-wave/boundary-layer interaction under the influence

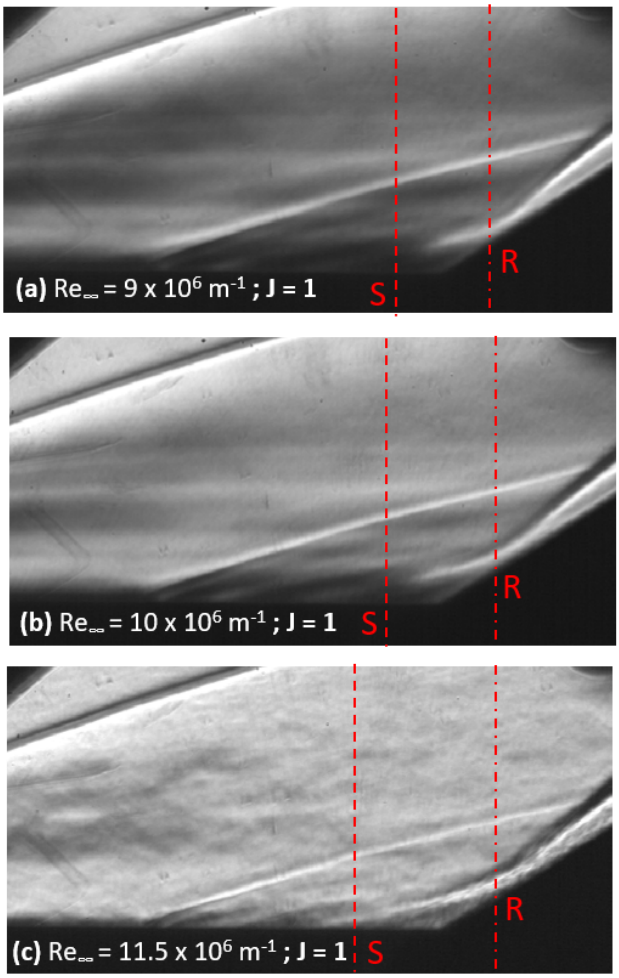

FIG 7. Schlieren visualisation of AJVG flow control at three Reynolds numbers. $J = 1$ for all cases.

of AJVGs at the two lower Reynolds numbers (Fig 7a and Fig 7b) are nearly similar to the undisturbed case. A precise quantification of the change in separation and reattachment lengths were not possible due to the changes being within the measurement uncertainty. However, considering that the 2D compression-ramp case shows a large reduction in separation length for a similar momentum flux ratio and flow Reynolds number ($Re_\infty = 9.6 \times 10^6 m^{-1}$; $Me = 2.5$; $J = 1.38$ [38]), the near constant behaviour in this axisymmetric interaction is rather surprising and requires further, more detailed investigation. With increase in flow Reynolds number to $Re_\infty = 11.5 \times 10^6 m^{-1}$, the separation length increases and an upstream movement of the separation shock wave is observed (see red dash line in Fig. Fig 7c). The decreased boundary layer thickness for high flow Reynolds numbers, coupled with increased AJVG injection pressure to attain $J = 1$, could have increased the obstruction effected by the jets resulting in the upstream moment of the separation shock. The location of the reattachment point R was nearly constant and within uncertainty limits for all three cases. Fig 8 shows the influence of momentum-flux-ratios on the separation lengths of the control cases, normalised with the respective lengths of the baseline case. The black line at $L_{sep} = 1$ denotes the baseline separation length. Note that, these lengths are extimated from schlieren images as the oil-flow separation lengths are not available for all the Reynolds numbers. It can be seen that, the other tested values of J (see Tab. 1) show the same trend at low values of momentum-flux ratio ($\sim J \leq 1$). However, at increasing values of J, the control effectiveness is seen to decreases for all the three tested flow Reynolds numbers

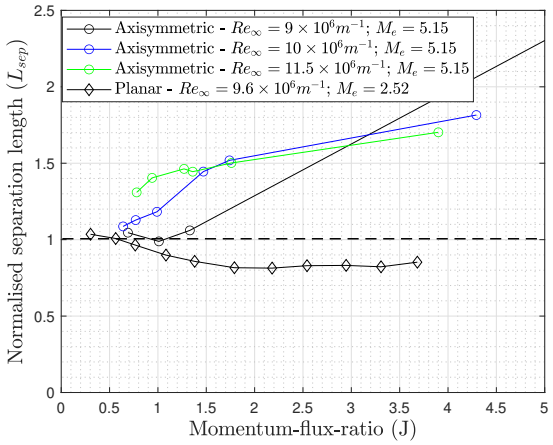

FIG 8. Normalised separation length vs momentum-flux-ratios for planar and axisymmetric configurations

Fig 8 also includes the influence of momentum-flux-ratio on the normalised separation lengths obtained for a planar shock-wave/boundary layer interaction under the influence of air-jet vortex generators of similar geometrical characteristics [22]. The contrast between the planar and axisymmetric configuration is clear, even at low momentum-flux coefficients. While almost all larger values of momentum-flux-ratios that were tested showed a significant reduction in separation length for the planar configuration, no such large scale separation length reduction was observed for the axisymmetric configuration. Although the two tested cases differ in Mach number, due to reasons discussed in section 3.3, we suspect that the reduced effectiveness might be related to the axisymmetric nature of the current configuration.

4. CONCLUSION

The effect of air-jet vortex generators (AJVGs) on an axisymmetric hypersonic shock-wave/boundary layer interaction was assessed for the first time in this investigation at $M_e = 5.15$. The uncontrolled baseline case was a 33^o flare-induced interaction. The global flow organisation and surface flow features were assessed using schlieren and oil-flow visualisation tools. Air-jets from circular orifices of 1 mm were injected in the spanwise direction, pitched at the angle of 45^o to the local surface tangent. Three different flow Reynolds numbers and various momentum-flux-ratios were tested in an attempt to investigate the effects of these parameters in an as large as possible range. A massive sep-

aration bubble was formed due to the adverse pressure gradient imposed by the 33^o flare on the incoming boundary layerx‘ and the overall structure of the separated flow was largely similar for the three tested flow Reynolds numbers.
Upon injection of the air-jets, an asymmetric system of streamwise vortices is generated, forming a streaky oil pattern downstream of the AJVG arrays. The boundary layer flow undergoes undulations in the azimuthal direction due to the presence of the streamwise vortices, resulting in the formation of the corrugated flow-separation line. The structure of the shock-wave boundary-layer interaction was largely unaltered at low values of momentum flux ratios (J) of the AJVG array and the interactions between the jet-induced vortices were weak such that the jets acted largely independently. Increasing the value of J increased the jet/jet interactions, which, based on investigations in 2D supersonic interactions, raised the expectation of an improved control efficiency. However, no large-scale downstream shift of the separation line was observed and the control effectiveness even decreases with increasing J due to large obstruction component of the jets. These observations may be related to the axisymmetric shape of the body and are currently the subject of further research. The flow Reynolds number had no significant effect on the control effectiveness at low Reynolds number; with increasing Reynolds number, the efficiency slightly weakened.
The relatively weak influence of AJVGs in the present configuration in comparison to 2D configuration at similar Re_∞ and J hints at the possible influence of axisymmetry on the control effectiveness. Further research on this aspect, as well as a detailed quantitative analysis using infrared thermography is currently underway to enable better understanding of the flow physics with and without control.

Acknowledgements:

This research was funded by the German Research Foundation (DFG) within the framework of the Emmy Noether Programme (grant SCHR 1566/1-1). Rolf Radespiel is gratefully acknowledged for providing us access to the HLB facility at ISM, TU Braunschweig. The contributions of Nick Capellmann and the workshop are gratefully acknowledged. The authors would also like to thank Maïlys Buquet and Arshad Alkireet for their valuable support.

Contact address:

d.ramaswamy@aia.rwth-aachen.de

References

[1] Holger Babinsky and John K. Harvey, editors. Shock Wave–Boundary-Layer Interactions. Cambridge University Press, 2011.

[2] Noel T. Clemens and Venkateswaran Narayanaswamy. Low-frequency unsteadiness of shock wave/turbulent boundary layer interactions. Annual Review of Fluid Mechanics, 46(1):469–492, January 2014.

[3] David S. Dolling. "fifty years of shock-wave/boundary-layer interaction research: What next?". AIAA Journal, 39(8):1517–1531, 2001.

[4] A.J. Smits and J.P. Dussauge. Turbulent Shear Layers in Supersonic Flow. American Institute of Physics, 1996. ISBN: 9781563962608.

[5] J. Delery and J. G Marvin. Shock-wave boundary layer interactions. AGARDograph, 1986. AGARD-AG-280.

[6] Jean M. Delery. Shock wave/turbulent boundary layer interaction and its control. Progress in Aerospace Sciences, 22(4):209–280, 1985.

[7] H. H. Pearcey. Shock Induced Separation and its Prevention by Design and Boundary Layer control. In G. V. Lachmann, editor, Boundary Layer and Flow Control, volume II, pages 1170–1355. Pergamon Press, 1961.

[8] John C Lin. Review of research on low-profile vortex generators to control boundary-layer separation. Progress in Aerospace Sciences, 38(4-5):389–420, May 2002.

[9] H. Babinsky, Y. Li, and C. W. Pitt Ford. Microramp control of supersonic oblique shock-wave/boundary-layer interactions. AIAA Journal, 47(3):668–675, 2009.

[10] Paul L. Blinde, Ray A. Humble, Bas W. van Oudheusden, and Fulvio Scarano. Effects of micro-ramps on a shock wave/turbulent boundary layer interaction. Shock Waves, 19(6):507–520, 2009.

[11] Anne-Marie Schreyer, Dipankar Sahoo, and Alexander Smits. Experiments on the influence of a microramp array on a hypersonic shock turbulent boundary layer interaction. In 41st AIAA Fluid Dynamics Conference and Exhibit. American Institute of Aeronautics and Astronautics, 2011.

[12] Mohd R. Saad, Hossein Zare-Behtash, Azam Che-Idris, and Konstantinos Kontis. Micro-ramps for hypersonic flow control. Micromachines, 3(2):364–378, April 2012.

[13] R. H. M. Giepman, F. F. J. Schrijer, and B. W. van Oudheusden. Flow control of an oblique shock wave reflection with micro-ramp vortex generators: Effects of location and size. Physics of Fluids, 26(6):066101, 2014.

[14] R. A Wallis. The use of air jets for boundary layer control, 1952. Aerodynamics notes 110.

[15] Ryszard Szwaba. Shock wave induced separation control by streamwise vortices. Journal of Thermal Science, 14(3):249–253, 2005.

[16] L. J. Souverein and J.-F. Debiève. Effect of air jet vortex generators on a shock wave boundary layer interaction. Experiments in Fluids, 49(5):1053–1064, 2010.

[17] R. A. Wallis and C. M. Stuart. On the Control of Shock-Induced Boundary Layer Separation with Discrete Air Jets, 1958. Aeronautical Research Council CP 595.

[18] Ryszard Szwaba. Influence of air-jet vortex generator diameter on separation region. Journal of Thermal Science, 22(4):294–303, 2013.

[19] J. P. Johnston and M. Nishi. Vortex generator jets - means for flow separation control. AIAA Journal, 28(6):989–994, 1990.

[20] S. B. Verma and C. Manisankar. Shockwave/boundary-layer interaction control on a compression ramp using steady micro jets. AIAA Journal, 50(12):2753–2764, 2012.

[21] R. Sebastian, T. Luerkens, and A-M. Schreyer. Flow field around a spanwise-inclined jet in supersonic crossflow. Accepted for publication in Aerospace Science and Technology, 2020.

[22] D. P. Ramaswamy, R. Hinke, and A.-M. Schreyer. Influence of jet spacing and injection pressure on separation control with air-jet vortex generators. In Notes on Numerical Fluid Mechanics and Multidisciplinary Design, pages 234–243. Springer International Publishing, 2019.

[23] S. B. Verma and C. Manisankar. Control of compression-ramp-induced interaction with steady microjets. AIAA Journal, 57(7):2892–2904, 2019.

[24] J. Kim, I. Bermejo-Moreno, A.-M. Schreyer, and J. Urzay. LES of hypersonic compression-corner flows with upstream sub-boundary-layer micro-ramp vortex generators. In Proceedings of the Summer Program, Center for Turbulence Research, Stanford University. 2016.

[25] A.-M. Schreyer, I. Bermejo-Moreno, J. Kim, and J. Urzay. Separation control in a hypersonic compression ramp interaction. In Proceedings of the Summer Program, Center for Turbulence Research, Stanford University. 2016.

[26] D. Sun, Q. Guo, C. Li, and P. Liu. Direct numerical simulation of effects of a micro-ramp on a hypersonic shock wave/boundary layer interaction. Physics of Fluids, 31(12):126101, 2019.

[27] R. Szwaba, P. Flaszyński, J.A. Szumski, and P. Doerffer. Influence of air cooling and air-jet vortex generator on flow structure in turbine passage. Task Quarterly, 19(2):153–166, 2015.

[28] M. Estrof, T. Wolf, and R. Radespiel. Experimental and numerical investigations on the operation of the hypersonic ludwieg tube braunschweig. In Fifth European Symposium on Aerothermodynamics for Space Vehicles, volume 563, page 579. American Institute of Aeronautics and Astronautics, 2005.

[29] Syed R. Ali, Jie Wu, Rolf Radespiel, Thomas Schilden, and Wolfgang Schroeder. High-frequency measurements of acoustic and entropy disturbances in a hypersonic wind tunnel. In 44th AIAA Fluid Dynamics Conference. American Institute of Aeronautics and Astronautics, 2014.

[30] J.D. Anderson. Modern Compressible Flow: With Historical Perspective. McGraw-Hill Education, 3rd edition, 2002.

[31] S. Stephan and R. Radespiel. Propulsive jet simulation in a hypersonic ludwieg tunnel. In Deutscher Luft- und Raumfahrtkongress, 2012.

[32] B. S. Stratford and G.S. Beaver. The Calculation of the Compressible Turbulent Boundary Layer in an Arbitrary Pressure Gradient - A Correlation of certain previous Methods, 1959. Aeronautical Research Council R. and M. No. 3207.

[33] Timothy Wadhams, Matthew MacLean, Michael Holden, and Eric Mundy. Pre-flight ground testing of the full-scale FRESH FX-1 at fully duplicated flight conditions. In 37th AIAA Fluid Dynamics Conference and Exhibit. American Institute of Aeronautics and Astronautics, 2007.

[34] Carson L. Running, Thomas J. Juliano, Joseph S. Jewell, Matthew P. Borg, and Roger L. Kimmel. Hypersonic shock-wave/boundary-layer interactions on a cone/flare model. In 2018 Fluid Dynamics Conference. American Institute of Aeronautics and Astronautics, 2018.

[35] Shibin Cao, Igor Klioutchnikov, and Herbert Olivier. Görtler vortices in hypersonic flow on compression ramps. AIAA Journal, 57(9):3874–3884, 2019.

[36] Guo-Lei Wang and Xi-Yun Lu. Effects of the jet-to-crossflow momentum ratio on a sonic jet into a supersonic crossflow. Theoretical and Applied Mechanics Letters, 1(1):012005, 2011.

[37] Anne-Marie Schreyer and Gonca Taskin. Separation control with lobe mixers in the wake of an axisymmetric space-launcher model. In New Results in Numerical and Experimental Fluid Mechanics XI. Notes on Numerical Fluid Mechanics and Multidisciplinary Design, vol 136. Springer, Cham. Dillmann A. et al. (eds), 2018.

[38] D. P Ramaswamy and A-M. Schreyer. Control of shock-induced boundary-layer separation using air-jet vortex generators. Accepted for publication in AIAA Journal, 2020.